Effective mass of conduction electrons in $Cd_{1-x}Mn_xTe$

Y. H. Matsuda,* T. Ikaida, and N. Miura
Institute for Solid State Physics, University of Tokyo 5-1-5 Kashiwanoha, Kashiwa, Chiba 277-8581, Japan

S. Kuroda, F. Takano, and K. Takita
Institute of Materials Science, University of Tsukuba 1-1-1 Tenoudai, Tsukuba, Ibaraki 305-8573, Japan
(Received 14 August 2001; published 15 February 2002)

Electron cyclotron resonance in $Cd_{1-x}Mn_xTe$ ($x=0$, 0.064, 0.097, 0.11) has been studied in high magnetic fields up to 150 T at photon energies in the range 44–117 meV. We found that the band-edge effective mass of the conduction electrons increases significantly with the Mn concentration. For comparison with the experimental results, the conduction-band Landau levels were calculated by means of the eight-band Pidgeon-Brown model taking into account the $s(p)$-d exchange interaction. The increase of the band gap due to the Mn ions alone is not sufficient to explain the observed enhancement of the mass. A possible reason for the mass enhancement is an effect of the sp-d hybridization. We also found that the electron mass decreases significantly with decreasing temperature. A large spin splitting of the Landau levels due to the exchange field qualitatively explains the relative temperature dependence of the mass.

DOI: 10.1103/PhysRevB.65.115202 PACS number(s): 76.40.+b, 75.50.Pp, 71.18.+y, 87.50.Mn

I. INTRODUCTION

Recently, use of the spin-dynamics degree of freedom has opened up possibilities for a new breed of devices. The new area is called *spintronics* and has attracted much attention from the point of view of both physics and practical applications. Diluted magnetic semiconductors (DMS's) are most promising materials for developing such new devices where the optical and electronic properties are controlled by applied magnetic fields through the exchange interaction, or the magnetic properties are changed by an applied bias voltage or irradiation with light.[1–3] Recent progress in the low-temperature epitaxial crystal growth technique enables the introduction of a large number of holes into semiconductors in order to make them ferromagnetic.[4–7] For the development of new DMS-based heterostructure devices, the knowledge of basic band parameters such as the effective mass and the g factor in DMS's is required.

However, accurate values for the band-edge mass of the free electrons and holes in DMS's have not been determined so far, even for the most thoroughly studied DMS, e.g., $Cd_{1-x}Mn_xTe$. This is partly because DMS's are generally low-mobility materials and it is very difficult to observe the cyclotron resonance (CR), i.e., to satisfy the condition $\omega_c\tau > 1$ (ω_c is the cyclotron frequency and τ is the relaxation time). Although the mobility becomes higher by lowering the temperature it is generally difficult to observe free carrier CR in bulk DMS samples, since most of the carriers are bound to impurities at low temperatures. The combination of low dimensionality and the $s(p)$-d exchange interaction results in a variety of interesting phenomena in the CR of DMS-based heterostructures.[8] The mobility of these samples is much larger than in bulk samples owing to the modulation doping technique.[8–10] However, the confinement potential introduced by the quantum structure significantly influences the effective mass through the band nonparabolicity and two-dimensional effects. This interferes with the evaluation of the effect of magnetic ions on the effective mass in the heterostructure samples.

DMS's have the interesting feature that they can be regarded as a prototype material of strongly correlated metals in the diluted limit. The band electrons are coupled strongly with the Mn ions through the sp-d hybridization,[11] and hole-mediated ferromagnetism can be induced by the strong p-d hybridization.[12] Since the effective mass of the band electrons in the strongly correlated metals such as the heavy fermion systems can deviate substantially from the free electron mass due to the interactions (in these materials the hybridization between $s(p)$ and localized $f(d)$ band plays an important role), one can envision that the effective mass of band electrons in DMS should be modified significantly by local magnetic ions in analogy with the strongly correlated metals. Although the many-body effect is generally not very significant in bulk semiconductors because of the small number of carriers, the strong coupling between conduction electrons (holes) and localized magnetic ions can give rise to a unique situation such as a magnetic (spin) polaron due to the $s(p)$-d exchange interaction.[13,14]

We have studied high-field cyclotron resonance up to 150 T in bulk $Cd_{1-x}Mn_xTe$ samples in order to determine the dependence of the electron effective mass on the Mn concentration. As a reference material, $Cd_{1-x}Mg_xTe$ was measured in order to compare the electron masses between magnetic and nonmagnetic compounds. $Cd_{1-x}Mg_xTe$ is important as a barrier material for the CdTe-based II-VI heterostructures such as CdTe/CdMgTe or CdMnTe/CdMgTe quantum wells.[8–10]

II. EXPERIMENTAL PROCEDURE

Pulsed magnetic fields up to 150 T are generated by the single-turn coil technique. The pulse duration is around 6 μs. Although the single-turn coil made of soft copper is destroyed by the Maxwell force in each experiment, the sample and the cryostat are not damaged because the de-

TABLE I. Characteristics of the samples used in this study. x denotes the Mn or Mg concentration, t is the thickness of the samples, and n_s and μ are the electron density and the mobility, respectively; these were obtained by Hall measurements at room temperature.

	$Cd_{1-x}Mn_xTe$				$Cd_{1-x}Mg_xTe$		
x	0	0.064	0.097	0.11	0.041	0.071	0.098
t (μm)	1	1	1	1	0.34	0.34	0.34
n_s (10^{17}cm^{-3})	6.2	2.0	0.88	7.2	20	18	20
μ (cm^2/Vs)	320	188	234	326	103	73	150

struction takes place only in the outwards direction.[15]

The He gas flow cryostat used in this work is made from thin bakelite tubes and caps. LORD 3170 (Lord Corporation) or STYCAST 1266 (ABLESTIK JAPAN) is used as a glue. (If we use STYCAST 1266 not only for a glue but also for the thin tubes and caps, we can make the cryostat made from the same material; it can avoid a strain induced by different contraction rates of the materials during the temperature decreases.[16]) The temperature can be changed from room temperature down to around 4 K.

Far-infrared radiation from CO_2 or H_2O lasers is used as the light source. The wavelengths used in this work are 10.6 μm (CO_2), 16.9 μm (H_2O), and 28 μm (H_2O). The radiation is applied as a pulse by using a mechanical chopper or by pulsed operation of the power supply of the laser. The 10.6-μm radiation was circularly polarized (electron-active direction). The pulse duration of the radiation is a few milliseconds for 10.6 μm and several tens of microseconds for 16.9 and 28 μm.

For 10.6 μm, we used a HgCdTe PIN-photodiode detector at 77 K (Kolmar Technologies, model KMPV11-1-B50) and for 16.9 and 28 μm a Ge:Cu photoelectric detector cooled by liquid He to near 4 K. The detectors and the amplifiers are operated by batteries and are located in a shielded box that is installed at a distance of $1\sim2$ m from the single-turn coil. The detector signal is converted to an optical signal by an optical transmitter (SONY Tektronics AS6900) connected to the transient recorder by a 20-m-long optical fiber. All recorders are installed in a screened room adjacent to the experimental room where the high field is generated.

The samples we measured in this work are $Cd_{1-x}Mn_xTe$ ($x=0$, 0.064, 0.097, 0.11) and $Cd_{1-x}Mg_xTe$ ($x=0.041$, 0.071, 0.098). All the samples were grown on GaAs (001) by MBE (molecular beam epitaxy) at the University of Tsukuba. Iodine is used as the dopant; all samples are n type. The Mn and Mg concentration x is determined by exciton photoluminescence (or reflectance) at 4.2 K and by x-ray diffraction. Properties of the samples are given in Table I.

III. RESULTS AND DISCUSSION

A. Dependence of CR on the Mn concentration at around 250 K

The magnetotransmission spectra of $Cd_{1-x}Mn_xTe$ ($x=0$, 0.064, 0.097, 0.11) at 10.6 μm and about 250 K are shown in Fig. 1. A single absorption peak due to the free electron cyclotron resonance is observed at about 100 T for each sample. This peak is found to shift towards higher fields as the Mn concentration increases; the effective mass increases with increasing x. The spectra are analyzed by a fitting procedure using a calculated transmission curve $T(B)$. We used the equation

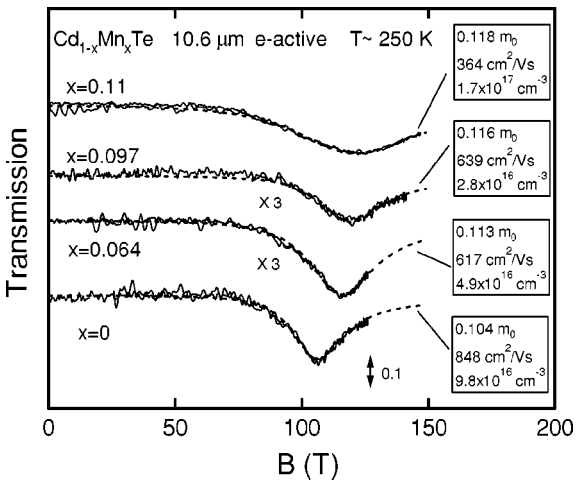

FIG. 1. Solid curves show the magnetotransmission spectra in $Cd_{1-x}Mn_xTe$ from the experiment. The dashed curves are the results of the line-shape analysis using a dielectric function. Cyclotron mass, cyclotron mobility, and carrier density, which are obtained by the analyses are also shown for each sample.

$$T=\frac{(1-R)^2\exp(-\kappa t)}{1-R^2\exp(-2\kappa t)}, \tag{1}$$

where R is the reflectivity, κ is the absorption coefficient, and t the thickness of the sample. The multi-interference effect was neglected (since the substrate was mechanically polished by hand, the surfaces of the sample plate were not parallel within the precision of 10 μm that would be needed to make this effect relevant for the wavelengths used in this work). R and κ are determined by the dielectric function ϵ that is given by

$$\epsilon=\epsilon_L+\frac{i}{\omega}\frac{\omega_p^2}{\omega_\tau-i(\omega\pm\omega_c)}, \tag{2}$$

where ϵ_L is the lattice dielectric constant, ω_τ is the relaxation rate, and ω_p is the plasma frequency. For the fitting procedure, we normalized the magnetotransmission with respect to the transmission at zero magnetic field: $T(B)/T(0)$. Since ω_p and ω_c are determined by the cyclotron mass m^*_{CR}, the carrier concentration n_s, and the relaxation rate ω_τ, we can calculate the change in transmission using Eqs. (1) and (2) where we take all three parameters as fitting parameters. As a result of the least-square-fitting calculation m^*_{CR}, n_s, and the cyclotron mobility $\mu(=e/\omega_\tau m^*_{CR})$ are obtained. In Fig. 1 the fitted curves of the transmission spectra are shown by dashed curves, together with values obtained from the fitting. The obtained mass is generally smaller than the value deduced directly from the absorption peak; this is caused by the rather

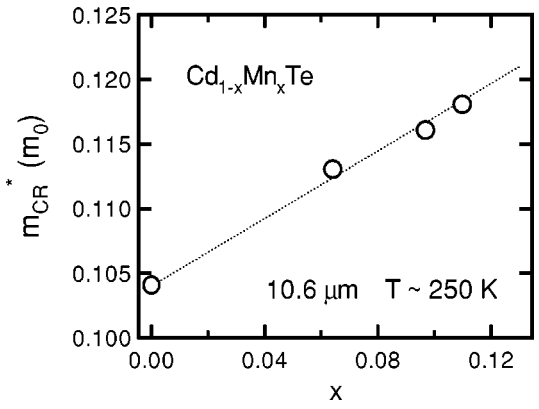

FIG. 2. Cyclotron masses obtained at 10.6μm (117 meV) at around 250 K are shown by open circles. The dotted line denotes the result of the least-square fit giving a relation $m^*_{CR}=[0.104+0.131x]\ m_0$.

broad CR absorption peak (for a sharp CR peak, the difference is usually negligible). The electron concentration obtained for all samples is 3–6 times smaller than the values obtained from the Hall measurement, while the mobility obtained from the CR is about three times larger than that given by the Hall measurement except for $x=0.11$ (see Table I). It is not yet certain why the electron concentration given by the CR spectrum is smaller; probably the freeze-out of carriers due to the high field decreases the electron density.

The cyclotron mass obtained at around 250 K is found to increase with x as shown in Fig. 2. The increase of the mass is roughly given by $m^*_{CR}=[0.104+0.131x]\ m_0$. (Here, it should be noted that the obtained mass increase is slightly smaller than the values reported in our previous reports,[17,18] where the cyclotron mass was deduced from the peak positions of the CR spectra directly without any line-shape analysis). As an approximate expression for the band-edge effective mass m^*, we can use the equation

$$\frac{m_0}{m^*}\sim\left(1+2\frac{P^2}{m_0E_g}\right), \tag{3}$$

where P is the momentum matrix element between the conduction and valence bands. According to this equation, m^* increases with E_g linearly as $2P^2/m_0 \gg E_g$. However, the observed increase of m^*_{CR} is much larger than expected from the increase of E_g given in the literature. The reported dependence of the band gap on x is $[1.516+1.26x]$ eV at room temperature and $[1.606+1.59x]$ eV at 4.2 K.[14,19] The observed rate of mass increase is $d(\ln m^*_{CR})/dx|_{x=0}=(1/\Delta x)\times\{\Delta m^*_{CR}/m^*_{CR}(x=0)\}\sim 1.25$, while the band gap increase rate is $d(\ln E_g)/dx|_{x=0}\lesssim 1$. This suggests that the x dependence of the band gap alone cannot explain the observed increase of the mass with x. We need a better model taking into account the effect of magnetic ions.

A theoretical study by Hui *et al.* suggests that the effective mass of electrons is affected considerably by the sp-d hybridization in DMS's;[20] this has been calculated by the $\boldsymbol{k}\cdot\boldsymbol{p}$ method, where the sp Hamiltonian matrix elements are effectively modified by the sp-d hybridization. These authors took 28 basis functions including the ten unoccupied upper and ten occupied lower d levels separated from each other by the on-site Coulomb energy, plus two s levels and six p levels. They proposed that the effect of the d levels can be introduced in an (8×8) $\boldsymbol{k}\cdot\boldsymbol{p}$ matrix for the sp band by a perturbation of order k^2. If the influence of the spin-orbit split-off band on the mass change due to the sp-d hybridization is small, the modification of P is the main part of the change in the sp Hamiltonian matrix. It is demonstrated in Ref. 20 that the effective masses of electrons and light holes in $Cd_{1-x}Mn_xTe$ increase with x due to this reduction in P. A strong reduction in P with increasing x has also been observed in $Hg_{1-x}Mn_xSe$.[21] In light of these considerations, the large difference between $d(\ln E_g)/dx|_{x=0}$ and $d(\ln m^*_{CR})/dx|_{x=0}$ in the present study strongly suggests that the reduction in P due to the sp-d hybridization really takes place in $Cd_{1-x}Mn_xTe$.

One may wonder if the band-gap is affected by many-body effects, e.g., band-gap renormalization, due to the rather high density of electrons in the samples, and whether the cyclotron mass may depend on the carrier density. In order to see the dependence of the CR on the electron density, we measured other $Cd_{1-x}Mn_xTe$ ($x=0.064$) samples with different carrier density, and found that the cyclotron mass obtained around 100 T is almost insensitive to the carrier density in the range of $n=2.0\times 10^{17}-6.7\times 10^{18}$ cm^{-3}. Moreover, as we show later on, the band-edge effective mass for CdTe obtained in the present work is in very good agreement with the literature value. Therefore, the band-gap renormalization does not have a significant effect in this case. The electron density is as large as the critical density of the Mott criterion ($n\sim 1.1\times 10^{17}$ cm^{-3} for CdTe).[22] However, at high magnetic fields the effect of the impurity band on the conduction band is expected to be small in the range of $10^{17}-10^{18}$ cm^{-3} because the spatial extension of the wave function is reduced by the high magnetic field. If the density exceeds 10^{19} cm^{-3}, the impurity band effect may show up. In fact, we observed the CR spectrum in CdTe with such a high density of electrons and found that the peak field as well as the shape of the entire transmission spectra are very different from those of other low-density samples. This effect will be discussed elsewhere.

Figure 3 shows the relation between the photon energy of the radiation and the CR transition fields. Since the cyclotron resonance in the present study is the quantum cyclotron resonance, we can deduce the cyclotron energy from the transition energy between the lowest two Landau levels; these can be calculated in terms of the eight-band Pidgeon-Brown (PB) model taking into account the $s(p)$-d exchange interaction.[23–26] The solid curves in Fig. 3 show the calculated inter-Landau-level transition energies as a function of magnetic field, where we used the standard set of Luttinger parameters for CdTe ($\gamma_1^L=5.3, \gamma_2^L=1.7, \gamma_3^L=2.0, \kappa^L=0.61$). The magnetization $\langle S_z\rangle$ was calculated by the modified Brillouin function taking the effective temperature $T_{eff}\sim T_{meas.}+2$ K.[27] As the measuring temperature $T_{meas.}$ is much higher than the temperature corresponding to the antiferromagnetic coupling between Mn ions ($J_{AF}\sim 7$ K), the effect

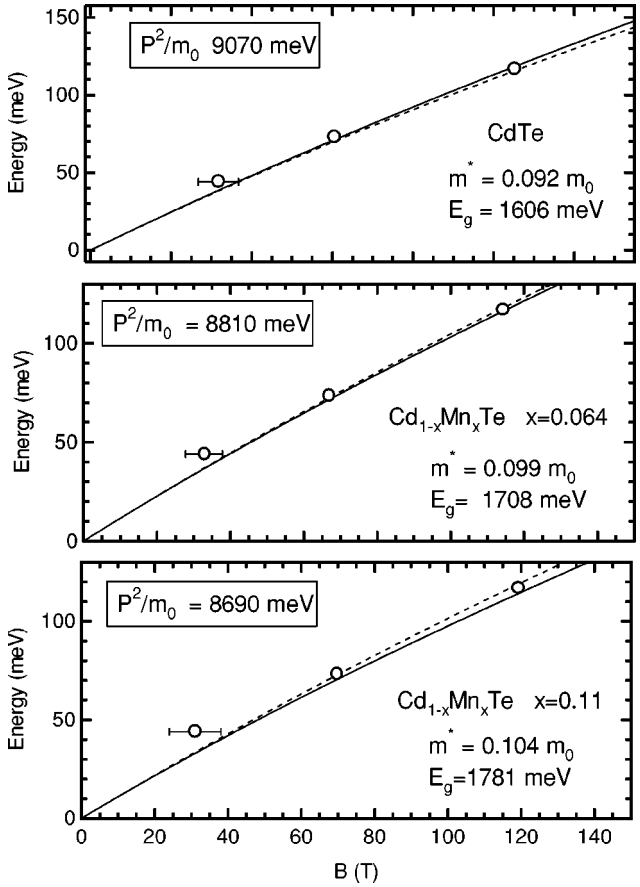

FIG. 3. Photon energy vs the CR transition fields for $Cd_{1-x}Mn_xTe$ ($x=0$, 0.064, 0.11). Open circles are the experimental results at around 250 K. Solid (dashed) curves denote the calculated inter-Landau-level transition energies between the $n=0$ and the $n=1$ Landau levels with spin-up (spin-down) states. The momentum matrix element P is taken as an adjustable parameter.

of the magnetization of the Mn clusters is not taken into account. We took the momentum matrix element P as an adjustable parameter in order to take into account the sp-d hybridization effect. P appears in the off-diagonal terms of the $\boldsymbol{k}\cdot\boldsymbol{p}$ Hamiltonian matrix [Eq. (B2) in Appendix B] for the modified PB model. We find that the results of the calculation reproduce the obtained CR positions well. We used the band-gap value at 4.2 K, $[1.606+1.59x]$ eV;[14] repeating the same calculation with the band-gap values at room temperature we found that the degree of the agreement of the fitting and the effective mass are almost the same. The band-edge mass m^* obtained by the fitting and the energy P^2/m_0 are plotted vs x in Fig. 4. The effective mass in $Cd_{1-x}Mn_xTe$ is found to be approximately given by the relation $m^*=[0.092+0.109x]m_0$; the effective mass for CdTe ($x=0$) is in good agreement with literature values ($0.090m_0$).[28] We also found that P is given by the relation $P^2/m_0=[9059-3495x]$ meV.

We can see a significant reduction of P with increasing x in Fig. 4. This reduction strongly suggests that the sp-d hybridization effect indeed plays an important role in enhancing the effective mass of the conduction electrons. Moreover, we found that the rate of increase of m^* and m^*_{CR} is consistent with the rate of mass increase given by Hui *et al.*,[20] when the sp-d hybridization is taken into account. Figure 5 shows the relative increase of the band-edge mass $[m^*(x)/m^*(0)$; open circles] and the cyclotron mass obtained at 10.6 μm $[m^*_{CR}(x)/m^*_{CR}(0)$; open squares] as a function of x. The solid and dashed lines denote the relative mass increase predicted by the theory.[20] These show the mass increase calculated with and without the sp-d hybridization effect. The mass increase deduced from the cyclotron resonance is in excellent agreement with the theoretical values based on the sp-d hybridization effect. Moreover, the recently observed electron CR in n-type $In_{1-x}Mn_xAs$ showed the possibility of the reduction of P due to the sp-d hybridization.[29]

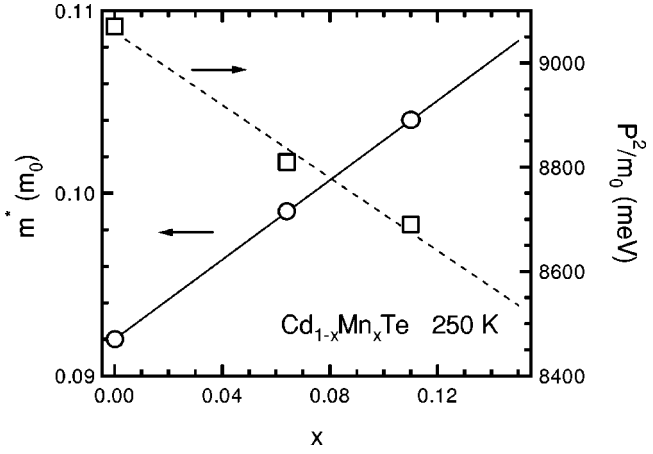

FIG. 4. Band-edge electron effective mass m^* (open circles) and momentum matrix element P (open squares) as a function of the Mn concentration x. The solid and dashed lines show the results of the least-square fit for m^* and P, respectively. These approximately follow the relations $m^*=[0.092+0.109x]\ m_0$ and $P^2/m_0=[9059-3495x]$ meV.

The sp-d hybridization effect may be closely related to

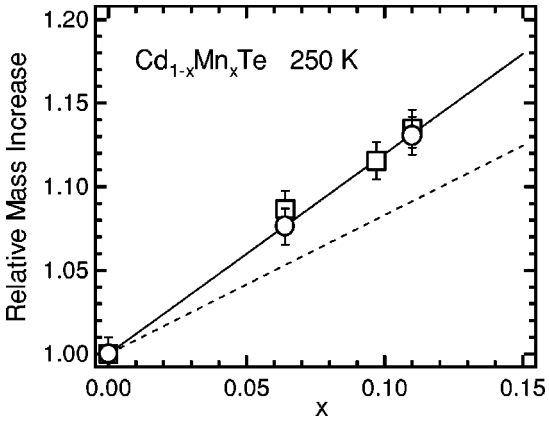

FIG. 5. Relative mass increase with the Mn concentration x. Open circles and open squares denote the experimental results for the band-edge mass and the cyclotron mass at 10.6 μm, respectively. Solid and dashed lines show the theoretical values deduced from Ref. 20; the solid line includes the sp-d hybridization effect, while the dashed line does not include the hybridization effect (only the band-gap effect is taken into account).

the physical situation of the anticrossing (or the repulsion) between the conduction band and the unoccupied *d* band (the upper Hubbard band of the Mn ion). The band repulsion due to the hybridization changes the dispersion relation of the bands, and thus the effective mass can be changed. The unoccupied *d* band is known to be above the conduction-band minimum by about 1.6 eV for $Cd_{1-x}Mn_xTe$. Although this energy is rather large by comparison to the energy region we are looking at in the conduction band, it is reasonable to expect some effects on the effective mass when the cyclotron energy is large enough.[18] A quantitative analysis with a better theoretical model is required to discuss this in more detail. On the other hand, we can imagine that the hole mass is influenced by the hybridization more significantly than the electron mass because the hybridization between the *p*-like valence band and the *d* band is usually much stronger than that between the *s*-like conduction band and the *d* band. In wide gap DMS's, e.g., ZnO-based and GaN-based DMS's that are predicted to become ferromagnetic even at room temperature,[12,30–32] the electron mass can be much enhanced by the hybridization since the unoccupied *d* band is near the conduction-band minimum. For instance, when we take the on-site Coulomb energy of the Mn ion to be ~ 7 eV (Ref. 11) and the band gap of ZnMnO to be 3.3 eV,[33] the expected energy difference between the unoccupied *d* band and the conduction-band minimum is ~ 0.3 eV. Therefore, it would be of interest to study the mass enhancement in these materials.

So far, we have not taken into account the polaron effect on the cyclotron mass. There should be some effect on the CR, in particular, at energies near the LO phonon energy (21 meV in CdTe). However, the resonant polaron effect may be negligible within our experimental error since the energy range of 44–117 meV is far away from the LO phonon energy. Hence, we believe that the polaron effect is negligibly small in this work. This assumption is supported by the fact that the electron band-edge mass in CdTe obtained in this study, i.e., $0.092m_0$, is closer to the literature value of the band-edge mass[28] $(0.090m_0)$ than that of the polaron mass $(0.096m_0)$.[34] It would be reasonable to assume that the polaron effect is insensitive to the Mn concentration as long as it is a small fraction.

B. Comparison between $Cd_{1-x}Mn_xTe$ and $Cd_{1-x}Mg_xTe$

The cyclotron masses of electrons in $Cd_{1-x}Mg_xTe$ at 10.6 μm and ~ 250 K are plotted vs x in the inset of Fig. 6. The dashed line is the result of the least-square fit that gives the relation $m^*_{CR}=[0.104+0.0956x]m_0$. The cyclotron mass was deduced from the line-shape analysis (CR spectra are not shown) as we did for $Cd_{1-x}Mn_xTe$ in the preceding section.

To compare the band-gap effect on the electron mass in $Cd_{1-x}Mn_xTe$ and $Cd_{1-x}Mg_xTe$, we plot the relative increase of the cyclotron mass, i.e., $\Delta m^*_{CR}(x)/m^*_{CR}(0)$ as a function of the relative increase of the band gap, i.e., $\Delta E_g(x)/E_g(0)$ for these two materials in Fig. 6. Here, we used $E_g=[1.52+1.26x]$ eV for $Cd_{1-x}Mn_xTe$ (Ref. 19) and $E_g=[1.52+1.67x]$ eV for $Cd_{1-x}Mg_xTe$.[35] The slope of relative mass

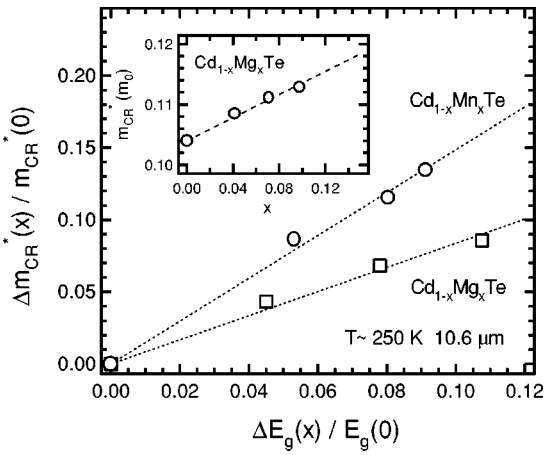

FIG. 6. Mass increase rate as a function of the rate of increase of the band gap. Open circles and open squares denote the rate of increase of the cyclotron mass for $Cd_{1-x}Mn_xTe$ and for $Cd_{1-x}Mg_xTe$, respectively. The dotted lines are the results of the least-square fit. In the inset the cyclotron masses obtained for $Cd_{1-x}Mg_xTe$ at 10.6 μm and ~ 250 K are plotted as a function of the Mg concentration. The mass increase is approximately given by $[0.104+0.0956x]$ m_0 as shown by the dashed line in the inset.

increase for $Cd_{1-x}Mg_xTe$ is found to be 0.84, while that for $Cd_{1-x}Mn_xTe$ is about 1.49; thus the mass enhancement is significantly larger in $Cd_{1-x}Mn_xTe$ than in $Cd_{1-x}Mg_xTe$.

When we neglect the first-hand term of the right-hand side of Eq. (3) the rate of mass increase [the slope of $\Delta m^*_{CR}(x)/m^*_{CR}(0)$ vs $\Delta E_g(x)/E_g(0)$, Fig. 6] should be about 1. Actually, the rate of mass increase obtained from the eight-band $\boldsymbol{k}\cdot\boldsymbol{p}$ calculation (PB model) taking only E_g as an adjustable parameter is found to be 0.81. This is very close to the value obtained for $Cd_{1-x}Mg_xTe$. This fact suggests that the mass increase in the nonmagnetic semiconductor $Cd_{1-x}Mg_xTe$ is mainly due to the increase of the band gap and that the reason for the unusually large mass enhancement in $Cd_{1-x}Mn_xTe$ is the effect of the *d* band of Mn ions.

C. Electron CR at low temperatures

The magnetotransmission spectra of $Cd_{1-x}Mn_xTe$ $(x=0.064)$ at various temperatures are shown in Fig. 7. The impurity-shifted cyclotron resonance (ICR) appears at lower fields than the free electron CR position at low temperatures. The ICR peak intensity increases with decreasing temperature; it reflects the freeze-out of free electrons. We also observed the ICR in other samples ($x=0$, 0.097, 0.11) and found almost the same behavior. The estimated ionization energy of the donor level is about 4–8 meV for all the samples that were studied.

We do not see any spin split CR in $Cd_{1-x}Mn_xTe$ ($x=0.064$, 0.097, 0.11). One of the reasons is that there are only few electrons in the spin-up $n=0$ Landau-level due to the large spin splitting of the Landau level induced by the $s(p)$-d exchange interaction. According to our Landau-level calculation for the $x=0.064-0.11$ samples, about 60–70 % of the electrons are expected to occupy the spin-down $n=0$ Landau level at 300 K and almost 100% at 50 K if we

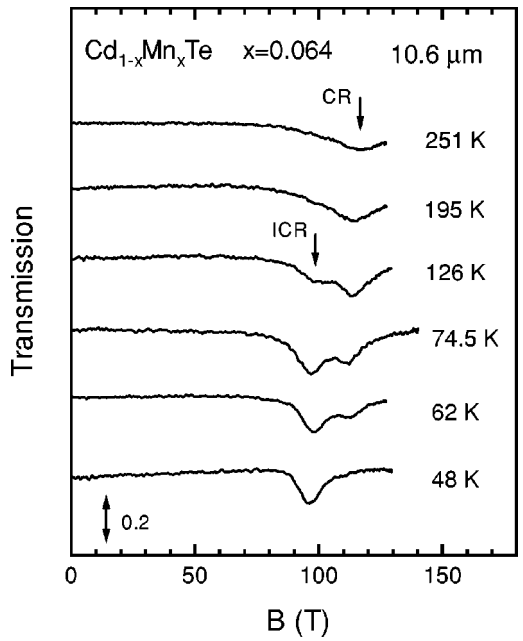

FIG. 7. Magnetotransmission spectra in $Cd_{1-x}Mn_xTe$ ($x=0.064$) at various temperatures. At low temperatures the impurity cyclotron resonance (ICR) appears at lower fields than the cyclotron resonance (CR) peak.

assume that all electrons are in the spin-up or spin-down $n=0$ Landau levels and that the occupation follows the Boltzmann distribution. On the other hand, the ratio of the electron population in the up and down $n=0$ Landau levels in CdTe is expected to be 7:3 even at 50 K. We show the representative calculated Landau levels in CdTe and $Cd_{1-x}Mn_xTe$ ($x=0.064$) at 60 K in Fig. 8.

Moreover, the difference between resonance positions corresponding to the spin-up and spin-down CR is expected

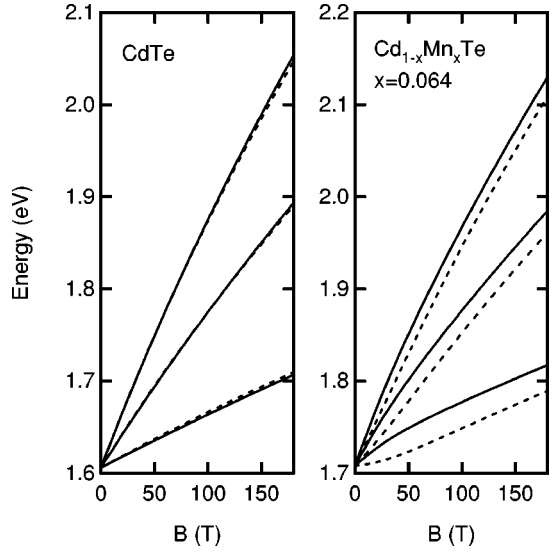

FIG. 8. Calculated conduction-band Landau levels in CdTe and those at 60 K in $Cd_{1-x}Mn_xTe$ ($x=0.064$). The solid and dashed curves denote the levels that originate from the spin-up and spin-down states, respectively.

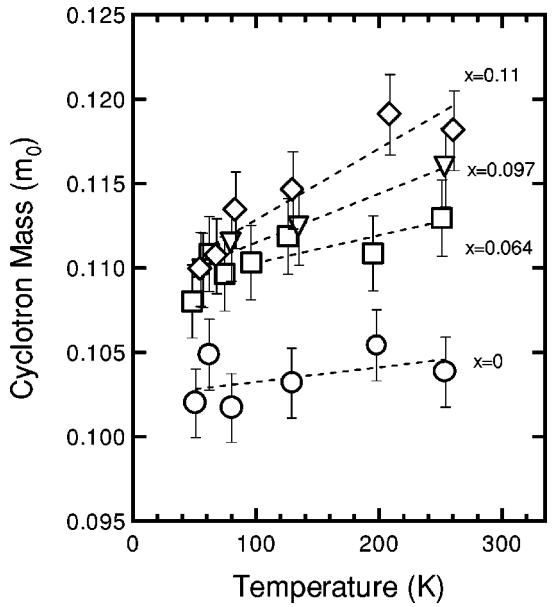

FIG. 9. Temperature dependence of the cyclotron masses at 10.6 μm in $Cd_{1-x}Mn_xTe$. The open circles, open squares, open triangles, and open diamonds are the results for the samples with $x=0$, $x=0.064$, $x=0.097$, and $x=0.11$, respectively. The dashed lines are the results of the least-square fit.

to be at most 5–10 T at 50 K and 1–5 T at room temperature; these are too small to be observed in the broad CR spectra obtained in this work. This small CR spin splitting seems to be unreasonable for $Cd_{1-x}Mn_xTe$ because the spin splitting of the Landau levels should be much larger than for CdTe. However, the degree of spin splitting of CR is not directly reflected by the degree of spin splitting of the Landau levels. It should be determined by the difference of the g factors between $n=0$ and $n=1$ Landau levels, i.e., the degree of the nonparabolicity of the band has to be considered. If the conduction band is parabolic, the Landau-level spin splitting should be the same for each Landau level, and the cyclotron transition energy is not expected to depend on the spin splitting of the Landau levels.

Figure 9 shows the temperature dependence of m^*_{CR} in $Cd_{1-x}Mn_xTe$ ($x=0$, 0.064, 0.097, 0.11) at 10.6 μm. The mass m^*_{CR} is found to decrease with decreasing temperature for each sample. The dashed lines are the results of the least-square fit. It can be seen that the temperature coefficient systematically increases with the Mn concentration. We can expect that the temperature dependence of the mass in CdTe is explained by the electron-phonon interaction[36] or by impurity related effects.[37] The temperature dependence of the mass is a rather complicated issue that is not yet well understood, especially in the range of megagauss fields and even in nonmagnetic semiconductors.[38] However, we can safely assume that the large temperature dependence of the mass increase obtained for $Cd_{1-x}Mn_xTe$ is due to the effect of magnetic ions. In Fig. 10(a), we plot m^*_{CR} at several temperatures as a function of x; this was deduced from the least-square fit in Fig. 9. The dotted curves are a guide for the eyes. We see a large temperature dependence in the mass enhancement, e.g., for $x=0.11$ we have 14% enhancement at

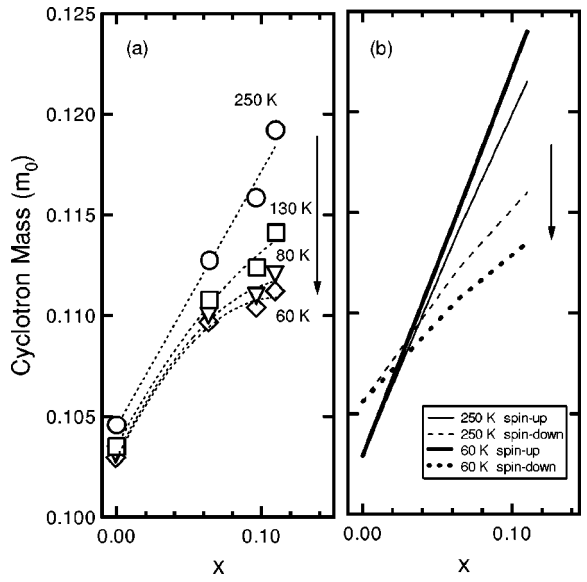

FIG. 10. (a) Cyclotron mass at 10.6 μm vs x at various temperatures. The masses are deduced from the temperature dependence of the cyclotron mass shown in Fig. 9. The open circles, open squares, open triangles, and open diamonds denote the masses at 250 K, 130 K, 80 K, and 60 K for each sample, respectively. (b) The calculated cyclotron masses using the Landau-level calculation at 250 K and 60 K. The arrows shown in (a) and (b) indicate the degree of mass decrease with decreasing temperature from 250 K to 60 K at $x=0.11$.

250 K but only 8% at 60 K. The calculated cyclotron masses using the modified PB model are plotted vs x in Fig. 10(b). The thin solid and dashed lines are spin-up and spin-down cyclotron masses for 250 K, while thick solid and dashed lines are the spin-up and spin-down cyclotron masses for 60 K. We can expect that the observed CR at 250 K is an envelope of the spin-up and spin-down CR, thus the obtained cyclotron mass is an averaged value. By contrast, we expect that the observed cyclotron mass at 60 K is the spin-up or spin-down cyclotron mass. We see that the dependence of m^*_{CR} on x seems to be linear at 250 K and to become nonlinear with decreasing temperature in Fig. 10(a); this fact can support our assumption. According to the calculated m^*_{CR} in Fig. 10(b), the averaged m^*_{CR} at 250 K changes linearly with x, while some nonlinear change in m^*_{CR} is expected at 60 K. Because the sign of the g factor for the $n=0$ Landau level changes from negative to positive with x due to the $s(p)$-d exchange interaction, the observed m^*_{CR} is the spin-up cyclotron mass at small x while it should be the spin-down cyclotron mass for large x (e.g., at 60 K the observed m^*_{CR} should be the spin-up mass for CdTe and that should be the spin-down mass for the $x=0.11$ sample). Therefore, we conclude that the large temperature dependence of m^*_{CR} observed for $Cd_{1-x}Mn_xTe$ can be explained qualitatively by the temperature-dependent spin splitting of the Landau levels and the electron population to those levels.

There still remain a few unsolved problems. First, the change in m^*_{CR} with temperature cannot be explained quantitatively by our calculation, e.g., the estimated degree of the calculated mass change is only 60% of that obtained by the experiment at $x=0.11$ as shown by the arrows in Figs. 10(a) and 10(b). Second, we have not taken into account the temperature dependence of E_g. All calculations were performed using the value of E_g at 4.2 K. The cyclotron mass apparently decreases with decreasing temperature, but E_g determined by an optical method increases with decreasing temperature, suggesting a mass increase with decreasing temperature. This behavior is completely opposite to our experimental results. Hence, we believe that the temperature dependence of E_g is not important to the electron mass at least at high fields in the megagauss range. More detailed theoretical models that include the electron-phonon interaction or some impurity effects will be required to solve these problems. We may also expect some effects of spin polarons on the electron mass at low temperatures.

IV. CONCLUSIONS

We found for the first time that the band-edge electron effective mass in $Cd_{1-x}Mn_xTe$ is significantly enhanced due to the presence of Mn ions. Based on a detailed comparison of the data with the eight-band modified Pidgeon-Brown model, the momentum matrix element P is found to decrease effectively with the Mn concentration. According to the theoretical study about the d-band effect on the sp Hamiltonian in the literature, the observed reduction of P can be due the sp-d hybridization. We also found that the mass increase in $Cd_{1-x}Mn_xTe$ is considerably larger than in $Cd_{1-x}Mg_xTe$. In the light of all these results, we conclude that not only the increase of the band gap but also the sp-d hybridization plays an important role for the enhancement of the electron mass. This information will be useful for developing new devices using magnetic semiconductors. The hole mass in the ferromagnetic p-type III-V DMS's, e.g., InMnAs and GaMnAs, or the electron mass in the wide gap DMS's, e.g., ZnO-based or GaN-based DMS's could also be affected by the strong sp-d hybridization.

The spin splitting of Landau levels due to the $s(p)$-d exchange interaction showed up in the large temperature dependence. Quantitative discrepancies in the temperature dependence of the cyclotron mass suggest that the electron-phonon interaction, the impurity effects, and possibly many-body effects can be important.

ACKNOWLEDGMENTS

We should like to thank Professor F. Herlach for valuable discussions and critical reading of the manuscript. This work was partially supported by a Grant-in-aid for Scientific Research on Priority Area "Spin Controlled Semiconductor Nanostructures" from the Ministry of Education, Science, Sports, and Culture.

APPENDIX A: ELECTRON CYCLOTRON RESONANCE IN HIGH MAGNETIC FIELDS

The condition for cyclotron resonance is given by

$$\hbar\omega = E_{n+1} - E_n (n=0,1,\ldots), \tag{A1}$$

where ω is the frequency of the radiation and E_n is the energy of the nth Landau level. The cyclotron mass m^*_{CR} is defined by

$$m^*_{CR}=\frac{eB}{\omega}, \tag{A2}$$

where B is the applied magnetic field. If the band is parabolic, m^*_{CR} is equal to the band-edge effective mass m^*, and it is independent of E_n.

However, when band nonparabolicity is introduced, the cyclotron mass depends on the energy E_n: m^*_{CR} generally increases with increasing Landau index n.

In high magnetic fields in the megagauss range (over 100 T) the lowest inter-Landau-level transition energy $\hbar\omega(=E_1-E_0)$ becomes $\sim$100 meV corresponding to a carrier density of the order of 10^{19} cm^{-3} for the effective mass $\sim 0.1m_0$ (m_0 is the free electron mass). Because of this large cyclotron energy, CR observed in the megagauss range is usually the inter-Landau-level transition from $n=0$ to $n=1$ (the system is in the quantum limit). Although there is a dispersion in the direction of the applied field (in the direction of k_z), almost all carriers should populate states at $k_z \sim 0$ due to the high density of states in high magnetic fields.

The cyclotron mass m^*_{CR} obtained in the high-field region is generally larger than the band-edge effective mass m^* due to the nonparabolicity. If we compare the energy dependence of m^*_{CR} with the calculated Landau levels, the band-edge effective mass m^* can be deduced as the zero energy limit of m^*_{CR}.

APPENDIX B: CALCULATION OF LANDAU LEVELS

For the calculation of the Landau levels, we used the eight-band $\boldsymbol{k}\cdot\boldsymbol{p}$ method in terms of the Pidgeon and Brown (PB) model.[23] This model treats the conduction band Γ^c_6 and the valence bands Γ^v_7,Γ^v_8 as quasidegenerate and accounts for the effect of the remote bands as a perturbation by means of several parameters. This model is well established for the narrow gap semiconductors such as InSb and InAs. The 14-band (five levels: Γ^c_6, Γ^c_7, Γ^c_8, Γ^v_7, Γ^v_8) $\boldsymbol{k}\cdot\boldsymbol{p}$ model will give the Landau levels more precisely as shown for GaAs and InP.[39] However, the 14-band $\boldsymbol{k}\cdot\boldsymbol{p}$ method makes the calculation too complicated if we treat the exchange interaction between electrons (holes) and Mn ions as matrix elements in addition to the ordinary set of Luttinger parameters. The gap between Γ^c_6 and Γ^c_7 is 3.77 eV in CdTe; this is not so much larger than the fundamental band gap, but it is still larger by a factor of 2.3. Moreover, as shown in Sec. III A, the observed cyclotron resonance positions for CdTe are well explained by the eight-band $\boldsymbol{k}\cdot\boldsymbol{p}$ model and the literature value of the band-edge mass of CdTe. Therefore, we believe that the eight-band model is sufficiently accurate to analyze the relative change in the mass arising from the Mn ions with respect to the effective mass of CdTe as a reference.

The set of the basis functions at the band extrema is

$$\Gamma_6\begin{cases} u_1=S\uparrow, \\ u_2=iS\downarrow, \end{cases}$$

$$\Gamma_8\begin{cases} u_3=\dfrac{1}{\sqrt{2}}(X+iY)\uparrow, \\ u_4=\dfrac{i}{\sqrt{2}}(X-iY)\downarrow, \\ u_5=\dfrac{1}{\sqrt{6}}[(X-iY)\uparrow+2Z\downarrow], \\ u_6=\dfrac{i}{\sqrt{6}}[(X+iY)\downarrow-2Z\uparrow], \end{cases} \tag{B1}$$

$$\Gamma_7\begin{cases} u_7=\dfrac{i}{\sqrt{3}}[-(X-iY)\uparrow+Z\downarrow], \\ u_8=\dfrac{1}{\sqrt{3}}[(X+iY)\downarrow+Z\uparrow], \end{cases}$$

where the symbols $\uparrow$ and $\downarrow$ stand for spin up and spin down, respectively. S is the conduction-band function that transforms as an atomic s-like function, and X, Y, Z are the valence-band functions that transform as atomic p_x-, p_y- and p_z-like functions, respectively. If we take the functions f_j as envelope functions, the zeroth-order wave function is given by $\Psi=\Sigma_j f_j u_j$. The matrix elements of the $\boldsymbol{k}\cdot\boldsymbol{p}$ Hamiltonian in the presence of the magnetic field can be written as an 8×8 matrix (D). Within first-order perturbation the matrix D is written in terms of two 4×4 matrices if we put $k_z=0$.

$$D=\begin{bmatrix} D_a & 0 \\ 0 & D_b \end{bmatrix}. \tag{B2}$$

The basis functions of the eigenvalue equations in matrix form

$$(D_a-\epsilon_a)f_a=0;\ \ (D_b-\epsilon_b)f_b=0 \tag{B3}$$

with the eigenvalues ϵ_a and ϵ_b are described in terms of harmonic-oscillator functions Φ_n,

$$f_a=\begin{pmatrix} a_1\Phi_n \\ a_3\Phi_{n-1} \\ a_5\Phi_{n+1} \\ a_7\Phi_{n+1} \end{pmatrix},\ \ f_b=\begin{pmatrix} a_2\Phi_n \\ a_6\Phi_{n-1} \\ a_4\Phi_{n+1} \\ a_8\Phi_{n-1} \end{pmatrix}. \tag{B4}$$

Then the determinantal equations for the eigenvalues of the a and b sets are expressed as given by Eqs. (17) and (18) in Ref. 23. (Some of the matrix elements should be slightly modified.)[24,25]

For the determinant equations in Ref. 23 the valence-band parameters γ_1, γ', γ'', and κ are used; these are different from the Luttinger parameters by the components corresponding to the interaction between the conduction and the valence bands.

In DMS's the exchange interaction between electrons (holes) and magnetic ions is introduced into the Hamiltonian using the mean-field approximation. The *sp-d* Hamiltonian can be described by the Heisenberg-like Hamiltonian $H_{sp\text{-}d} = \Sigma_j J(\mathbf{r}-\mathbf{R}_j)\mathbf{s}\cdot\mathbf{S}_j$, with $\mathbf{S}_j$ and $\mathbf{s}$ standing for spin operators of the j th Mn ion and the band electron (hole), respectively. The matrix elements of the *sp-d* Hamiltonian with the basis functions given by Eq. (B1) are obtained as an additional matrix D',[26]

$$D' = N_0 \begin{bmatrix} D'_a & D'_c \\ D'^{\dagger}_c & D'_b \end{bmatrix}, \tag{B5}$$

where

$$D'_a = \begin{bmatrix} \frac{1}{2}\alpha S_{zj} & 0 & 0 & 0 \\ 0 & \frac{1}{2}\beta S_{zj} & 0 & 0 \\ 0 & 0 & -\frac{1}{6}\beta S_{zj} & -\frac{i\sqrt{2}}{3}\beta S_{zj} \\ 0 & 0 & \frac{i\sqrt{2}}{3}\beta S_{zj} & \frac{1}{6}\beta S_{zj} \end{bmatrix}, \tag{B6}$$

and

$$D'_b = \begin{bmatrix} -\frac{1}{2}\alpha S_{zj} & 0 & 0 & 0 \\ 0 & \frac{1}{6}\beta S_{zj} & 0 & \frac{i\sqrt{2}}{3}\beta S_{zj} \\ 0 & 0 & -\frac{1}{2}\beta S_{zj} & 0 \\ 0 & -\frac{i\sqrt{2}}{3}\beta S_{zj} & 0 & -\frac{1}{6}\beta S_{zj} \end{bmatrix}. \tag{B7}$$

Here, $\alpha = J_{\Gamma_6} = \langle S|J|S\rangle$ and $\beta = J_{\Gamma_8} = \langle X|J|X\rangle$; these are the exchange interaction constants for an electron and for a hole, respectively. N_0 is the number of the cation sites in the volume of a unit cell.

For a paramagnetic state only the S_z component of the localized spin of the magnetic ion remains nonzero after averaging. Since all terms in the matrix D'_c are proportional to $(S_{xj} \pm iS_{yj}) \times (sp\text{-}d$ exchange constant), all of them vanish for the paramagnetic $Cd_{1-x}Mn_xTe$ samples studied in this work. Hence, there remain only 4×4 matrices in Eq. (B5), i.e., D'_a and D'_b, thus we have two 4×4 matrices $D_a + D'_a$ and $D_b + D'_b$ for the calculation.

At high magnetic fields in the megagauss range, the magnetic length ($l_c = \sqrt{\hbar/eB}$) becomes very small, e.g., $l_c = 26$ Å and 8.1 Å at 100 T and 1000 T, respectively. The effective-mass theory would break down if the wave-function extension of the electrons decreases to a size that is comparable with the periodic length of the lattice potential. However, at around 100 T, $2l_c$ is still an order of magnitude larger than the lattice constant of the popular cubic semiconductors such as GaAs or CdTe. Also, it is larger than the average distance between the Mn^{2+} ions, even at the lowest concentration used in our experiments ($\sim$10 Å for $x = 0.064$). Hence, the $\boldsymbol{k}\cdot\boldsymbol{p}$ method still functions well in this magnetic-field range.

*Electronic address: ymatsuda@issp.u-tokyo.ac.jp

[1] H. Ohno, Science **281**, 951 (1998).

[2] S. Koshihara, A. Oiwa, M. Hirasawa, S. Katsumoto, Y. Iye, C. Urano, H. Takagi, and H. Munekata, Phys. Rev. Lett. **78**, 4617 (1997).

[3] H. Ohno, D. Chiba, F. Matsukura, T. Omiya, E. Abe, T. Dietl, Y. Ohno, and K. Ohtani, Nature (London) **408**, 944 (2000).

[4] H. Munekata, T. Penney, and L.L. Chang, Surf. Sci. **267**, 342 (1992).

[5] H. Ohno, H. Munekata, T. Penney, S. von Molnar, and L.L. Chang, Phys. Rev. Lett. **68**, 2664 (1992).

[6] H. Ohno, A. Shen, F. Matsukura, A. Oiwa, A. Endo, S. Katsumoto, and Y. Iye, Appl. Phys. Lett. **69**, 363 (1996).

[7] F. Matsukura, H. Ohno, A. Shen, and Y. Sugawara, Phys. Rev. B **57**, R2037 (1998).

[8] Y. Imanaka, T. Takamasu, G. Kido, G. Karczewski, T. Wojtowicz, and J. Kossut, Physica B **298**, 392 (2001).

[9] S. Scholl, J. Gerschutz, F. Fischer, A. Waag, K. Schull, K. Schafer, and G. Landwehr, Solid State Commun. **94**, 935 (1995).

[10] G. Karczewski, J. Jaroszynski, A. Barcz, M. Kutrowski, T. Wojtowicz, and J. Kossut, J. Cryst. Growth **184/185**, 814 (1998).

[11] B.E. Larson, K.C. Hass, H. Ehrenreich, and A.E. Carlsson, Phys. Rev. B **37**, 4137 (1988).

[12] T. Dietl, H. Ohno, F. Matsukura, J. Cibert, and D. Ferrand, Science **287**, 1019 (2000).

[13] P.A. Wolff, in *Semiconductors and Semimetals*, edited by J. K. Furdyna and J. Kossut (Academic Press, New York, 1988), Vol. 25, p. 413.

[14] J.K. Furdyna, J. Appl. Phys. **64**, R29 (1988).

[15] K. Nakao, F. Herlach, T. Goto, S. Takeyama, T. Sakakibara, and N. Miura, J. Phys. E **18**, 1018 (1985).

[16] S. Takeyama, K. Amaya, T. Nakagawa, M. Ishizuka, K. Nakao, T. Sakakibara, T. Goto, N. Miura, Y. Ajiro, and H. Kikuchi, J. Phys. E **21**, 1025 (1988).

[17] Y.H. Matsuda, N. Miura, S. Kuroda, M. Shibuya, and K. Takita, J. Cryst. Growth **214/215**, 400 (2000).

[18] Y.H. Matsuda, N. Miura, S. Kuroda, M. Shibuya, K. Takita, and A. Twardowski, Physica B **294/295**, 467 (2001).

[19] P. Lautenschlager, S. Logothetidis, L. Vina, and M. Cardona, Phys. Rev. B **32**, 3811 (1985).

[20] P.M. Hui, H. Ehrenreich, and K.C. Hass, Phys. Rev. B **40**, 12 346 (1989).
[21] S. Takeyama and R.R. Galazka, Phys. Status Solidi B **96**, 413 (1979).
[22] C. Leighton, I. Terry, and P. Becla, Phys. Rev. B **58**, 9773 (1998).
[23] C.R. Pidgeon and R.N. Brown, Phys. Rev. **146**, 575 (1966).
[24] R.S. Kim and S. Narita, Phys. Status Solidi B **73**, 741 (1976).
[25] M.H. Weiler, in *Semiconductors and Semimetals*, edited by R.K. Willardson and A. C. Beer (Academic Press, New York, 1981), Vol. 16, p. 119.
[26] J. Kossut, in *Semiconductors and Semimetals*, edited by J.K. Furdyna and J. Kossut (Academic Press, New York, 1988), Vol. 25, p. 183.
[27] N. Kuroda and Y.H. Matsuda, in *Proceedings of the 25th International Conference on the Physics of Semiconductors, Osaka, Japan, 2000*, edited by N. Miura and T. Ando (Springer, Berlin, 2001), p. 272.
[28] M. Helm, W. Knap, W. Seidenbusch, R. Lassnig, and E. Gornik, Solid State Commun. **53**, 547 (1985).
[29] Y.H. Matsuda, T. Ikaida, N. Miura, M.A. Zudov, J. Kono, and H. Munekata, Physica E **10**, 219 (2001).
[30] K. Sato and H. Katayama-Yoshida, Jpn. J. Appl. Phys., Part 2 **39**, L555 (2000).
[31] K. Sato and H. Katayama-Yoshida, Jpn. J. Appl. Phys., Part 2 **40**, L334 (2001).
[32] K. Sato and H. Katayama-Yoshida, Jpn. J. Appl. Phys., Part 2 **40**, L485 (2001).
[33] T. Fukumura, Z. Jin, A. Ohtomo, H. Koinuma, and M. Kawasaki, Appl. Phys. Lett. **75**, 3366 (1999).
[34] A.L. Mears and R.A. Stradling, Solid State Commun. **7**, 1267 (1969).
[35] S.G. Choi, Y.D. Kim, S.D. Yoo, D.E. Aspnes, I. Miotkowski, and A.K. Ramdas, Appl. Phys. Lett. **71**, 249 (1997).
[36] W. Xiaoguang, F.M. Peeters, and J.T. Devreese, Phys. Rev. B **36**, 9765 (1987).
[37] J.T. Devreese, V.M. Fomin, V.N. Gladilin, Y. Imanaka, and N. Miura, Physica B **214/215**, 465 (2000).
[38] H. Yokoi, S. Takeyama, N. Miura, and G. Bauer, Phys. Rev. B **44**, 6519 (1991).
[39] P. Pfeffer and W. Zawadzki, Phys. Rev. B **53**, 12 813 (1996).